

# Impact of AlN Seed Layer on Microstructure and Piezoelectric Properties of $Y_xAl_{1-x}N$ ( $x = 15\%$ ) Thin Films

Shardul Pandit,\* Michael Schneider, Claudio Berger, Sabine Schwarz, and Ulrich Schmid

Alloying transition metals into aluminum nitride (AlN) has surged over the past decade to increase the piezoelectric performance of AlN for microelectromechanical systems (MEMS) applications. So far, the highest piezoelectric coefficients have been achieved by alloying scandium into AlN. But, most recently published studies have theoretically predicted by ab-initio calculations that yttrium can also be a promising and less expensive alternative to scandium. This paper focuses on the impact of an AlN seed layer on the growth and piezoelectric properties of sputter-deposited, polycrystalline  $Y_{0.15}Al_{0.85}N$  thin films on a silicon substrate. For the first time, the increase in piezoelectric performance of  $Y_xAl_{1-x}N$  ( $x = 15\%$ ) thin films with a  $d_{33}$  of  $\approx 7.85$  pC N<sup>-1</sup> due to this seed layer approach is presented, thus reaching in good agreement theoretical predictions. Furthermore, for the first time, the crystalline stability of  $Y_{0.15}Al_{0.85}N$  layers in a pure oxygen environment up to 1200 °C is reported, demonstrating a high oxygen resistance up to 800 °C even in this harsh environment. Detailed thin film analysis is done with various techniques such as X-ray diffraction, atomic force microscopy, nano-indentation, and high-resolution transmission electron microscopy and correlated with piezoelectric coefficient measurements.

its compatibility with conventional CMOS technology,<sup>[1–4]</sup> excellent high-temperature stability, a high Curie temperature of  $T_C = 1150$  °C, a high thermal conductivity up to  $285$  W m<sup>-1</sup> K<sup>-1</sup><sup>[5]</sup> and a high chemical resistance.<sup>[6]</sup> It has been integrated as an active layer in various MEMS sensor applications such as viscosity and density sensors<sup>[1–7]</sup> or smoke particle detectors,<sup>[8]</sup> micro speakers,<sup>[9]</sup> micro mirrors,<sup>[10]</sup> and ultrasonic transducers.<sup>[11]</sup> AlN has also successfully been implemented in micromachined energy harvester applications.<sup>[12]</sup> A low permittivity  $\epsilon_r \approx 10$ <sup>[6]</sup> and a high sound velocity ( $v_s \approx 6000$  m s<sup>-1</sup>) make AlN one of the best choices for surface and bulk acoustic wave resonator devices in modern communication applications.<sup>[13]</sup> Despite these advantages, AlN features only moderate piezoelectric coefficients  $d_{33} \approx 4 - 6$  pC N<sup>-1</sup><sup>[1–6]</sup> and therefore novel approaches are needed to overcome this drawback.

## 1. Introduction


The outstanding future market potential is predicted for silicon microelectromechanical systems (MEMS) based on piezoelectric thin film technology.<sup>[1]</sup> Although having a polycrystalline microstructure due to the moderate substrate temperatures during sputter deposition, the group III–V material aluminum nitride (AlN) has shown a strongly growing impact over the last decade, especially for sensing and filter applications.<sup>[2,3]</sup> This is due to many outstanding material properties, such as

Based on ab initio predictions, the benefit of additional alloying elements into pure AlN to achieve increased piezoelectric properties were proposed by different research groups in the last decades. Ternary systems based on scandium<sup>[14–16]</sup> or chromium,<sup>[17]</sup> as well as quaternary systems applying alloying elements such as zirconium, hafnium,<sup>[18]</sup> or niobium<sup>[19]</sup> in combination with, for example, magnesium, have been extensively studied. The highest  $d_{33}$  of 27.6 pC N<sup>-1</sup> in an AlN-based material system as of yet has been achieved experimentally by alloying AlN with 43 at% scandium.<sup>[14]</sup> However, a major drawback of scandium is its scarcity and, thus, high price, which can vary between several thousand and several ten thousand dollars per kilogram. In addition, the wurtzite structure in scandium alloyed with AlN (ScAlN) required for piezoelectricity is theoretically only thermodynamically stable up to a scandium concentration of 50 at%.<sup>[14]</sup> In contrast, Yttrium has a similar electronic outer shell configuration compared to scandium. Therefore, researchers have studied yttrium alloying into AlN through ab initio calculations.<sup>[20–23]</sup> Yttrium alloyed with AlN (YAlN) is predicted to reach similar or even higher values for  $d_{33}$  of up to 35 pC N<sup>-1</sup> for 50 at% of yttrium, as the wurtzite structure in YAlN is predicted to be stable up to yttrium concentrations of 75 at%.<sup>[20]</sup> As an added benefit, yttrium is significantly cheaper compared to scandium, as the scandium metal cost per kilogram is 100 times higher than that of yttrium.<sup>[24]</sup>

Theoretical works previously reported by Tholander et al.<sup>[21]</sup> presented diverging results on the impact of yttrium alloying

S. Pandit, M. Schneider, C. Berger, U. Schmid  
Institute of Sensor and Actuator Systems  
TU Wien  
Gusshausstrasse 27–29, Vienna A-1040, Austria  
E-mail: shardul.pandit@tuwien.ac.at

S. Schwarz  
University Service Center for Transmission Electron Microscopy  
(USTEM)  
TU Wien  
Wiedner Hauptstrasse 8–10/057-02, Vienna 1040, Austria

 The ORCID identification number(s) for the author(s) of this article can be found under <https://doi.org/10.1002/aelm.202200789>.

© 2022 The Authors. Advanced Electronic Materials published by Wiley-VCH GmbH. This is an open access article under the terms of the Creative Commons Attribution License, which permits use, distribution and reproduction in any medium, provided the original work is properly cited.

DOI: 10.1002/aelm.202200789

into AlN compared to those done by Mayrhofer et al.<sup>[22]</sup> and Manna et al.<sup>[23]</sup> Therefore, there is a strong need for experimental investigations of YAlN to exploit the full potential of this promising high-performance material system. Zukauskaitė et al.<sup>[20]</sup> presented experimental results on the microstructure but not on the piezoelectricity of  $Y_xAl_{1-x}N$  thin films. Mayrhofer et al.<sup>[22]</sup> were the first to present experimentally measured piezoelectric coefficients in polycrystalline  $Y_xAl_{1-x}N$  but could not demonstrate an improvement compared to sputter-deposited pure AlN thin films due to an amorphous oxygen-rich interface layer which formed at the onset of film growth at the interface to the silicon substrate. Compared to pure AlN thin films, most recently, Schlögl et al.<sup>[25]</sup> demonstrated for the first time in agreement with density functional theory (DFT) calculations  $Y_{0.09}Al_{0.91}N$  thin films which were reactively magnetron sputter-deposited without a seed layer on silicon with increased piezoelectric coefficients of  $d_{33} = 7.79 \text{ pm V}^{-1}$  by applying a pre-alloyed YAl compound target.<sup>[22]</sup> Both Mayrhofer et al.<sup>[22]</sup> and Schlögl et al.<sup>[25]</sup> faced severe technological challenges due to the presence of oxygen in the deposited  $Y_xAl_{1-x}N$  thin films. This was attributed either to oxygen contamination in the deposition chamber<sup>[22–25]</sup> or to significant oxygen concentrations in the targets, especially when manufactured by powder metallurgical sintering.<sup>[25]</sup> This indicates that both low residual oxygen in the deposition chamber and oxygen-free targets are two key requirements of utmost importance to achieve high quality and hence, piezoelectric  $Y_xAl_{1-x}N$  thin films. The oxygen issue is addressed by a careful selection of the fabrication process used for the alloyed target. Furthermore, to achieve a higher degree of *c*-axis orientation, a seed layer prior to the  $Y_{0.15}Al_{0.85}N$  deposition and based on a pure AlN film is introduced. The AlN seed layer provides the crystallographic information for the growing  $Y_{0.15}Al_{0.85}N$  film, thus supporting the incorporation of the large yttrium atoms into the crystal lattice at its defined sites. This approach is stimulated by similar studies reporting enhanced crystallographic properties for ScAlN,<sup>[26–28]</sup> but has not been investigated for YAlN thin film so far.

It is the objective of this study to evaluate the impact of a pure, 45 nm thin AlN seed layer on the quality and piezoelectric properties of  $Y_{0.15}Al_{0.85}N$  thin films. We utilize reactive sputtering from an arc-melted Y/Al alloy target for film synthesis and investigate the impact on both the *c*-axis orientation and the corresponding piezoelectric constants of  $Y_{0.15}Al_{0.85}N$  thin films. We analyze the deposited layers with X-ray diffractometry (XRD), selected area electron diffraction (SAED) imaging, and high-resolution transmission electron microscopy (HR-TEM). We also discuss the thermal stability of  $Y_{0.15}Al_{0.85}N$  thin films when subjected to high temperatures of up to 1200 °C in a pure oxygen environment. To the best of the authors' knowledge, this is the first study reporting experimental results for piezoelectric constants of  $Y_{0.15}Al_{0.85}N$  thin films matching those of theoretical ab initio predictions.

## 2. Experimental Details

$Y_{0.15}Al_{0.85}N$  thin films are realized from a Y/Al alloy target from AJA International, Inc., having a purity of 99.9% with

**Table 1.** Atomic percentage of Y and Al in a sputter-deposited YAl thin film by EDX (first column) and in the arc melted target as provided by the manufacturer (second column).

Element	at% (EDX)	at% (datasheet)
Yttrium	14.8	15.0
Aluminum	85.2	85.0

a fixed concentration of 15 at% yttrium. The diameter of the target is 150 mm. The alloy target is manufactured using an arc-melting process, ensuring the highest purity, especially concerning the oxygen content, as we will discuss below. These films are synthesized in a DC magnetron sputtering equipment LS730S from Von Ardenne, which is not a co-sputtering tool, but a standard sputtering system with a planar geometry comparable to those used in semiconductor industry. (100) p-type silicon wafers with 100 mm diameter serve as substrates.

Yttrium shows a high affinity toward oxygen.<sup>[29]</sup> Therefore, to estimate the oxygen concentration within the arc-melted target, a  $Y_{0.15}Al_{0.85}$  thin film with a thickness of 3 μm was sputter-deposited in a pure argon atmosphere. This thin film is investigated with energy dispersive X-ray spectroscopy (EDX) within a scanning electron microscope (SEM). The accelerating voltage was 20 keV. **Table 1** shows the measured Y and Al atomic concentrations of the film. The measured concentrations are in good agreement with the nominal values of the Y/Al alloy target, as provided by the manufacturer. The oxygen concentration in the YAl thin film was below the detection limit of the EDX system.

The base pressure before starting the deposition is below  $10^{-7}$  mbar. For the deposition experiments, both Al and  $Y_{0.15}Al_{0.85}$  targets were simultaneously installed in the same vacuum chamber and used either for the pure AlN seed layer or the  $Y_{0.15}Al_{0.85}N$  thin film deposition, respectively. According to the parameters given in **Table 2**, these targets are pre-sputtered for cleaning purposes as well as for conditioning the vacuum chamber of the sputter system. To remove any native oxygen present on the Si wafers, they were dipped in buffered hydrofluoric acid, rinsed with acetone and isopropanol, and subsequently subjected to inverse sputter etching (ISE parameters are given in Table 2) prior to deposition.<sup>[6]</sup> Next, on one of the two silicon wafers, an AlN seed layer with a thickness of 45 nm is deposited before  $Y_{0.15}Al_{0.85}N$  synthesis according to the parameters given in Table 2. The  $Y_{0.15}Al_{0.85}N$  thin film with a thickness of 1110 nm is realized on both substrates with a substrate temperature of  $\approx 350$  °C. Additional parameters are provided in Table 2. Radiative substrate heating is applied for 3600 s prior to  $Y_{0.15}Al_{0.85}N$  thin film deposition to stabilize the substrate temperature.

## 3. Characterization Methods

To determine crystal orientation, a Malvern PANalytical X'pert PRO X-ray powder diffractometer was applied for XRD analysis with a Copper tube operating at 45 and 40 kV and a current of 40 mA. The wavelength of the X-rays is 1.540598 Å for  $K\alpha_1$  and

**Table 2.** Sputtering parameters applied for pre-sputtering and for the deposition of YAlN thin films.

	Inverse sputter etching	Al target cleaning	Y/Al target conditioning	AlN seed layer deposition parameters	YAlN deposition parameters
Pressure [ $\mu$ bar]	6	3	3	4	4
Power [W]	200	300	300	800	800
Target substrate distance [mm]	88	65	65	65	65
Argon flow [sccm]	60	0	0	0	0
Nitrogen flow [sccm]	0	50	50	50	50
Estimated temperature of Substrate heating [ $^{\circ}$ C]	0	0	0	0	350
Time [s]	30	4000	8000	90	3600

1.544426 Å for  $K\alpha_2$ . The sample-to-source distance was 140 mm, and the detector had an active length of  $2.546^{\circ}$ . First, a Bragg–Brentano scan was measured from  $20^{\circ}$  to  $80^{\circ}$  to identify the crystallographic phases present in the film. In addition, rocking curves are also recorded for the (002) peak of  $Y_{0.15}Al_{0.85}N$ . The rocking curve range was selected from  $34^{\circ}$  to  $38^{\circ}$  as the (002) peak maximum can be found in this range. To estimate the high-temperature resistance of the  $Y_{0.15}Al_{0.85}N$  thin films, XRD measurements in a 100 % oxygen environment were performed. The equipment chamber for high-temperature XRD is an Anton Paar HTK 1200 N. The pressure of oxygen was kept at 1 atmosphere with a flow rate of  $0.4 \text{ L min}^{-1}$ . During this experiment, the temperature was varied from 27 to 1200  $^{\circ}$ C, and Bragg–Brentano and rocking curves were continuously measured. Also, to study the crystallographic phase stability of  $Y_{0.15}Al_{0.85}N$ , temperatures of 700, 800, and 900  $^{\circ}$ C were maintained for 24 h while continuously performing Bragg–Brentano scans.

The detailed microstructure investigation of two samples was subjected to cross-sectional high-resolution transmission electron microscopy (HR-TEM). For this purpose, an FEI TECNAI F20 at an operating voltage of 200 kV was applied. The orientation and crystallographic phase identification were made by selected area electron diffraction (SAED). The image processing was performed with Digital Micrograph.

The surface topology of the  $Y_{0.15}Al_{0.85}N$  thin films is analyzed using an atomic force microscope (AFM) Dimension Edge from Bruker. An n-doped Si cantilever was selected, having a spring constant of  $42 \text{ N m}^{-1}$ , which resulted in a resonance frequency of 320 kHz. The image processing was done in Gwyddion.

Fischer–Cripps Laboratories UMIS nano-indenter equipped with a Berkovich diamond tip was used for nano-indentation. This method allows us to determine Young's modulus of  $Y_{0.15}Al_{0.85}N$ . The films labeled as AY (i.e., with AlN as the seed layer) and with Y (i.e., without AlN as the seed layer) were subjected to a decrementing indentation force starting from 30 mN with a decrement of 0.5 mN per indent over 30 indents per sample.

The piezoelectric constant  $d_{33}$  was measured with a Piezometer PM300 from Piezotest Ltd., with a direct loading approach. For sample preparation, a shadow mask was used that allowed the simultaneous deposition and patterning of Al contact pads with a diameter of 1000  $\mu$ m and thickness of 300 nm. The backside of the substrate was fully coated with Al again with a thickness of 300 nm.

## 4. Results and Discussion

### 4.1. XRD Analysis

#### 4.1.1. Bragg–Brentano and Rocking Curves

The predominantly *c*-axis-oriented pure aluminum nitride shows a pronounced (002) peak around  $36^{\circ}$ , being characteristic of the presence of the wurtzite microstructure of AlN. **Figure 1** shows the scans for both  $Y_{0.15}Al_{0.85}N$  samples. The Y sample features a pronounced (002) peak with reference to AlN, but a significant increase in (002) peak intensity is observed for the AY sample with an integrated AlN seed layer. This indicates a higher degree of crystallinity in the AY sample compared to the Y sample. Peaks near  $32^{\circ}$  correspond to the (100) plane in AlN and  $Y_{0.15}Al_{0.85}N$ . The higher intensity of (100) in the Y sample indicates a few grains oriented in the desired *c*-axis orientation. The impact of these properties on the piezoelectric response is discussed in Section 4. The small peak observed from the AlN and the AY samples at  $34.5^{\circ}$  are due to the presence of tungsten in the XRD chamber after prolonged use. The peak at  $33^{\circ}$  represents the (100) reflection peak of the Si substrate.

The shift in peaks observed in **Figure 1** can be justified by the induced stress due to the yttrium atom into the wurtzite crystal. Therefore, the film with the AlN seed layer (AY sample) helps to optimize the stress and align it more to the (002) axis. Rocking curves for the films are measured for the (002) peak of both sample configurations. The full-width-at-half-maximum (FWHM) of the rocking curves is  $2.7^{\circ}$  for the AY sample and  $72^{\circ}$  for the Y sample as compared to the  $1.9^{\circ}$  for pure AlN. This confirms the poor crystal orientation in the Y sample as compared to the AY sample.

#### 4.1.2. High-Temperature XRD Measurements

For the temperature-dependent XRD measurements, only the AY sample was investigated, as the Y sample had a considerably poor FWHM of the rocking curve. **Figure 2a** shows XRD measurement results around  $2\theta = 36^{\circ}$  in Bragg–Brentano configuration from 25 to 1200  $^{\circ}$ C in a pure oxygen atmosphere. The AY sample features a high-intensity peak at  $35.90^{\circ}$  (at 100  $^{\circ}$ C) up to 800  $^{\circ}$ C, whereas above, the intensity drops as the  $Y_{0.15}Al_{0.85}N$  layer starts to lose its crystallographic (002) phase. It can also be observed that the peak starts to shift

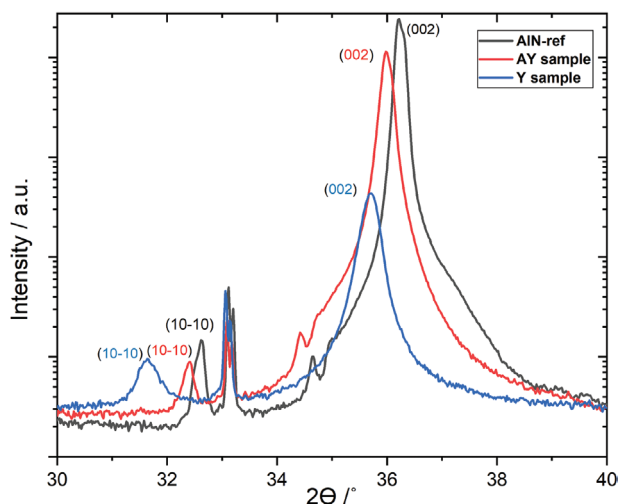


**Figure 1.** XRD characteristics of both the Y and AY samples in Bragg–Brentano mode with reference to AlN.

towards lower angles by  $-0.12^\circ$  as the wurtzite crystal enlarges due to thermal expansion. The thermal expansion coefficient of AlN is  $\alpha_{||} = 3.48 \times 10^{-6} \text{ K}^{-1}$  corresponding to a shift in  $2\theta$  by  $-0.09^\circ$ , which is in excellent agreement with observation.<sup>[30]</sup>

Latest above  $900^\circ\text{C}$ , the in-diffusion of oxygen, most probably in parallel with the out-diffusion of nitrogen, leads to an amorphization of the originally polycrystalline microstructure in combination with a strong change in the chemical layer composition.<sup>[31]</sup> As the sample did not show the (002) crystallographic phase above  $900^\circ\text{C}$ , 24 h high-temperature stability tests were conducted again in a pure oxygen atmosphere at  $700^\circ\text{C}$ ,  $800^\circ\text{C}$ , and  $900^\circ\text{C}$  to study the long-term oxygen resistance under such harsh environmental conditions. The corresponding Bragg–Brentano scans for these temperatures are given in Figure 2b–d, respectively. In Figure 2b,c, the corresponding (002) peaks are stable over the entire 24 h of temperature load. However, as shown in Figure 2d, at  $900^\circ\text{C}$ , the crystallographic (002) phase in  $\text{Y}_{0.15}\text{Al}_{0.85}\text{N}$  starts to disappear after 1 h and is almost completely gone after about 2 h. For pure AlN, M. Gillinger et al.,<sup>[31]</sup> observed a similar behavior at  $1000^\circ\text{C}$ , where the (002) peak disappears after about 2 h.<sup>[31]</sup> For ScAlN, similar investigations were performed,<sup>[32,33]</sup> demonstrating its crystalline stability at high temperatures up to  $1000^\circ\text{C}$ .<sup>[32]</sup> This research work demonstrates, for the first time, that although the oxidation resistance is reduced in  $\text{Y}_{0.15}\text{Al}_{0.85}\text{N}$  compared to pure AlN, it is still sufficiently high for most of the semiconductor device fabrication process steps as well as during device operation for a large range of application scenarios.

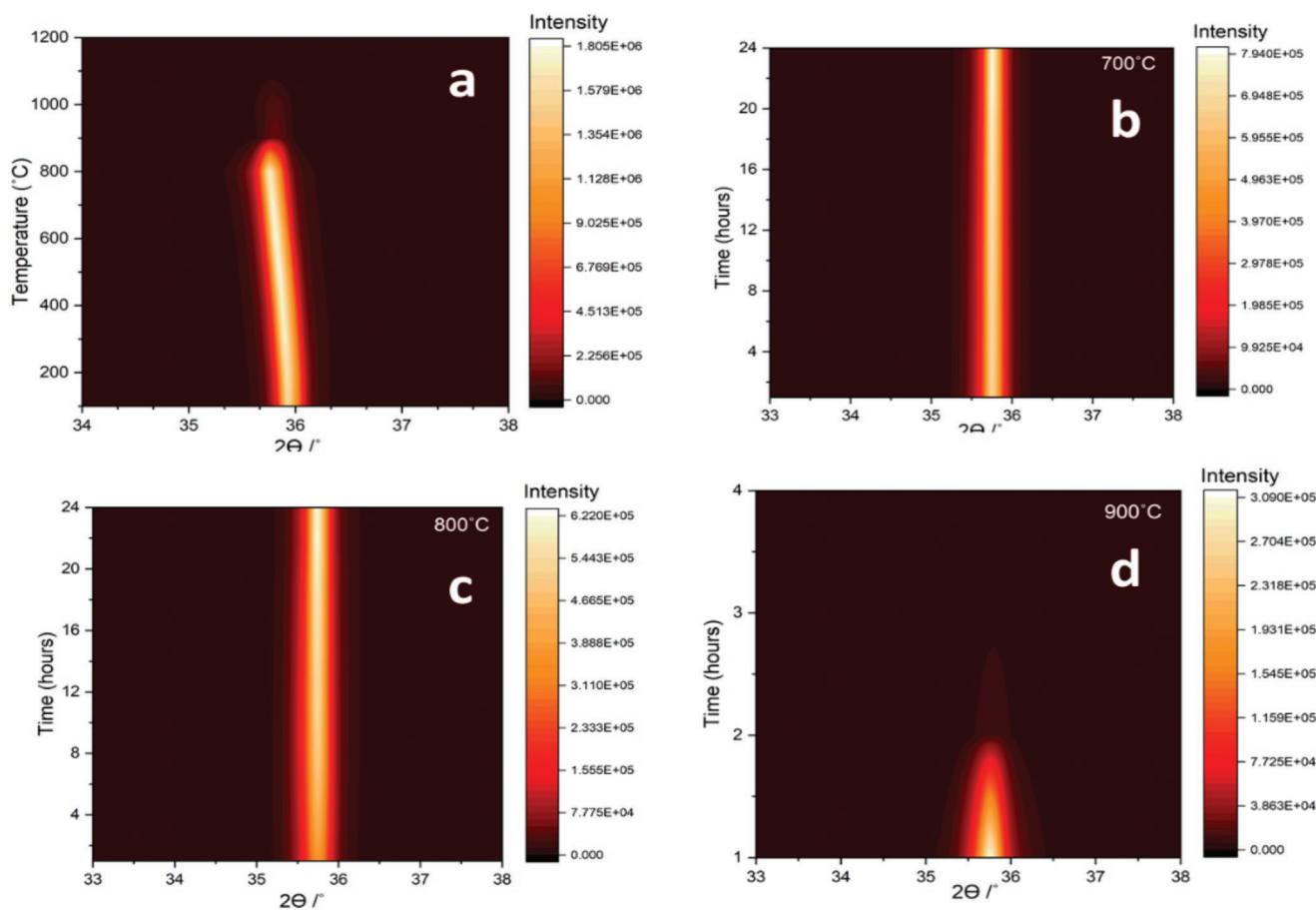


**Figure 2.** a) Bragg–Brentano scan of the AY sample from 25 to  $1200^\circ\text{C}$ , b) Bragg–Brentano scan at  $700^\circ\text{C}$ , c) Bragg–Brentano scan at  $800^\circ\text{C}$ , and d) Bragg–Brentano scan at  $900^\circ\text{C}$ .

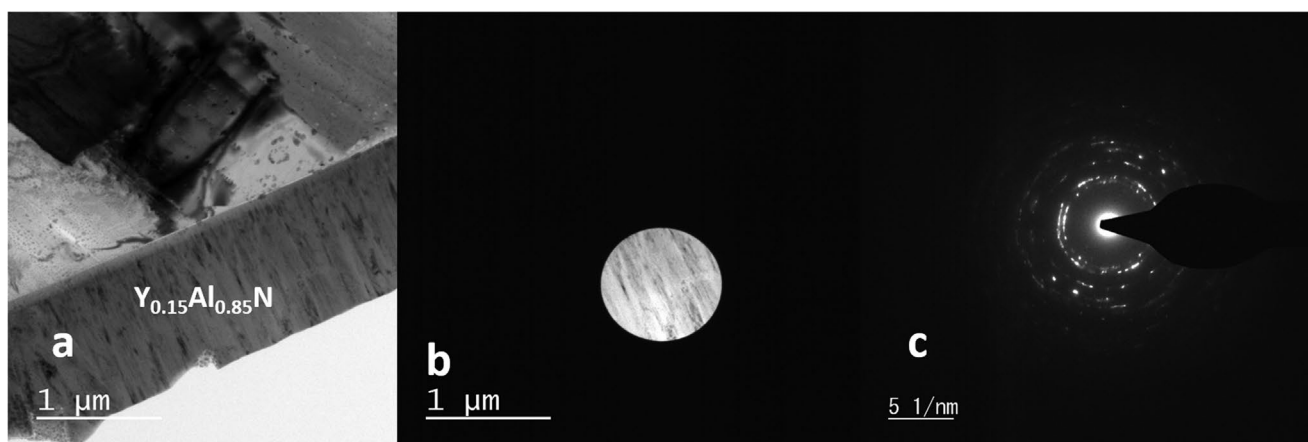


**Figure 3.** TEM cross-sectional analysis and selected area electron diffraction (SAED) of the Y sample.

To study in detail the microstructure of  $Y_{0.15}Al_{0.85}N$ , both the Y sample and the AY sample are subjected to cross-sectional HR-TEM analyses. **Figure 3a** gives an overview of the Y sample in a cross-sectional view, whereas **Figure 3b** illustrates the area selected by the aperture in the thin film for electron diffraction. This area is chosen to encompass the central part of the film. **Figure 3c** shows the selected area electron diffraction measurement of the Y sample. The image does not show a regular reciprocal lattice which would be expected for highly *c*-axis-orientated films. **Figure 4** shows high-resolution bright-field images of the same sample at different levels of magnification. Close to the interface, a highly irregular crystalline structure is observed. A visible difference, in contrast, is observed in **Figure 4a,b** by TEM imaging, as the contrast aperture cuts out higher spatial frequencies of the Fourier transform of the real space object allowing the amorphous phases to appear brighter. This is in agreement with the low-intensity peak gained from Bragg-Brentano analysis and in the high FWHM value of the rocking curve, respectively. **Figure 4a–c** illustrates, due to the higher resolution, the presence of the misoriented grains in the Y sample even more clearly.

A similar high-resolution TEM study was performed for the AY sample. Given the significantly higher crystalline quality, SAED was performed in addition to studying the impact of the AlN seed layer on  $Y_{0.15}Al_{0.85}N$  film quality at different positions

in the substrate and across the film thickness. **Figure 5a** shows the cross-section of the AY sample. **Figure 5a** also indicates the selected areas for SAED across the cross-section of the sample. As a reference, **Figure 5b** shows the SAED measurement of the silicon substrate, where the peak indices in the gray color can be clearly identified by the bright, distinct spots. In **Figure 5c**, the area including both silicon and the AlN seed layer is selected, and the resulting peak indices of (002) AlN (in red) can be identified, proving an excellent wurtzite crystallographic microstructure on the Si substrate, as expected for AlN on ISE pre-treated silicon substrates.<sup>[4]</sup> In **Figure 5d**, an area encompassing the silicon substrate, AlN seed layer, and  $Y_{0.15}Al_{0.85}N$  is chosen. Therefore, the resulting electron diffraction image shows the corresponding diffraction peaks from all three materials. The indices of Si (gray) and AlN (red) are continued from **Figure 5c**, while the brighter spots in the (002) plane (in yellow) demonstrate that the  $Y_{0.15}Al_{0.85}N$  thin film grows in a wurtzite structure as the AlN seed layer. **Figure 5e,f** shows the selected middle and upper regions in  $Y_{0.15}Al_{0.85}N$ , resulting in bright and sharp spots of the peaks corresponding to the (002) orientation, which demonstrates the excellent wurtzite crystal quality of  $Y_{0.15}Al_{0.85}N$  grown on AlN seed layers.

**Figure 6a–d** highlights the high-resolution image showing the properly oriented grain microstructure of the AY sample. These results are in excellent agreement with the high intense

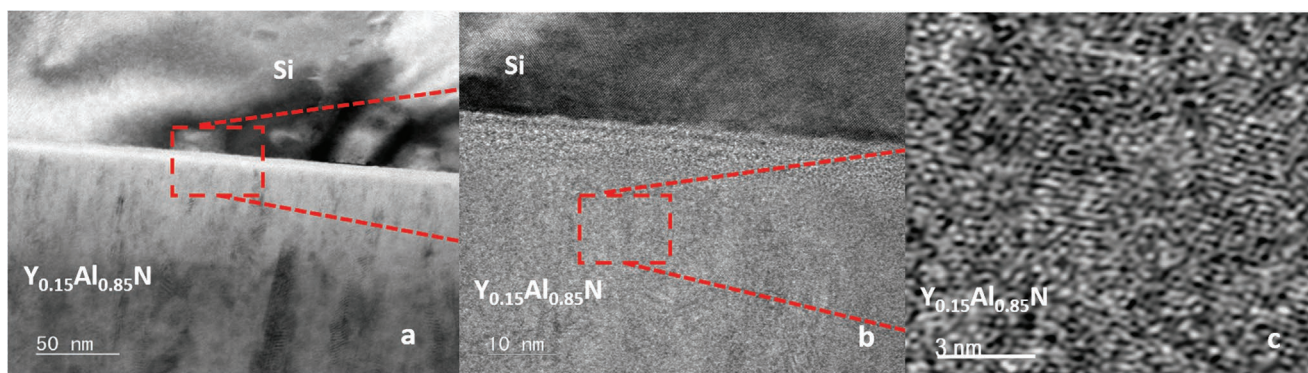


**Figure 4.** High-resolution transmission electron microscopy (HR-TEM) imaging of the Y sample.

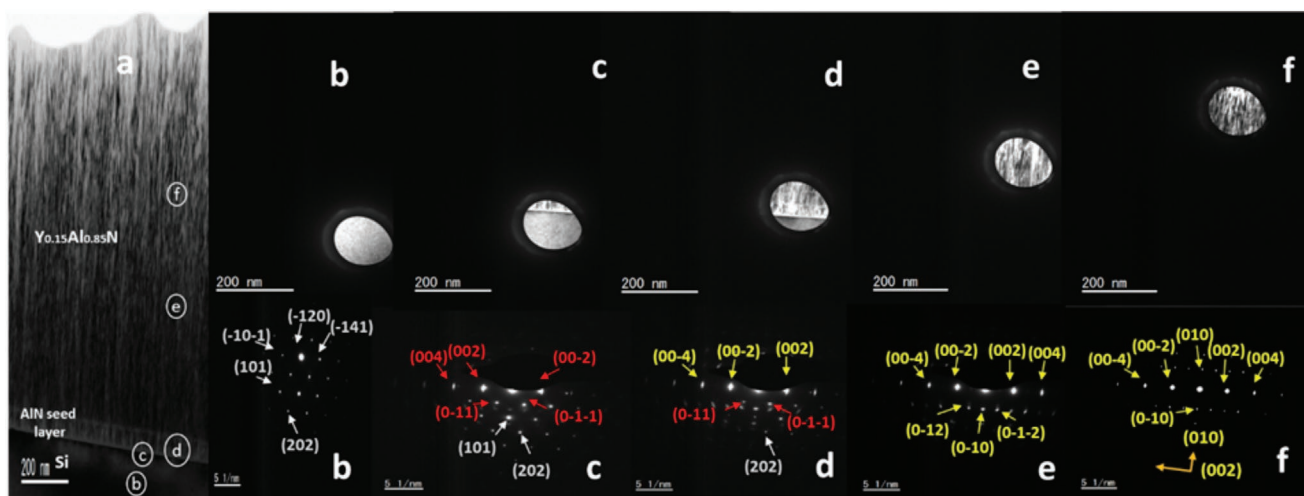


**Figure 5.** Cross-sectional TEM and SAED analyses at different positions of the AY sample. The crystallographic lattice indices of Si, AlN, and  $Y_{0.15}Al_{0.85}N$  are given in gray, red, and yellow colors, respectively.

XRD peak characteristics and the corresponding low FWHM determined from rocking curves of the AY sample.

**Figure 7** shows the surface topography of the AY sample with an RMS roughness of about 1.50 nm across a scan area of  $1 \times 1 \mu m^2$ . The lateral mean grain size is calculated from valley-to-valley distances in line scans with Gwyddion. They are observed to be closely packed with an average grain size of about 34 nm.

In contrast, the grains in the Y sample are randomly shaped and have a larger grain size, as can be observed in **Figure 8**. The RMS roughness is 3.50 nm across a scan area of  $1 \times 1 \mu m^2$ . The average grain size of about 134 nm is substantially larger compared to the AY sample.

Akiyama et al.,<sup>[34]</sup> performed the grain study on ScAlN and concluded that the grain size is important to achieve a large piezoelectric response, as a smaller grain size can result in a lower roughness of the thin film and consequently in a higher value of  $d_{33}$ .

The Young's modulus determined from the nano-indentation of both samples is shown in **Figure 9**. The mean value for the AY sample is  $249 \pm 5.6$  GPa, and the mean value of the Y sample is  $232 \pm 12.3$  GPa. Both values obtained from the mechanical characterization are in good agreement with the theoretical predictions of 235 GPa made by Mayrhofer et al.,<sup>[22]</sup> and 260 GPa by Manna et al.,<sup>[23]</sup> while no significant difference is observed in Young's moduli of the two  $Y_{0.15}Al_{0.85}N$  films due to the presence or absence of the AlN seed layer.

Theoretical ab initio calculations made by Mayrhofer et al., predict an increase of the piezoelectric constant with the increase in alloying of yttrium into AlN, similar to the theoretical and experimental behavior of scandium-alloyed with AlN. The  $d_{33}$  value is estimated to 7.5–8  $pm V^{-1}$  for  $Y_{0.15}Al_{0.85}N$  compared to 5  $pm V^{-1}$  for pure AlN.<sup>[22]</sup>

The size of the measured sample was  $1.5 \times 1.5 cm^2$ . The Y sample featured a  $d_{33}$  value of  $2.45 pC N^{-1}$ . This low value was expected due to the large FWHM and low crystalline quality

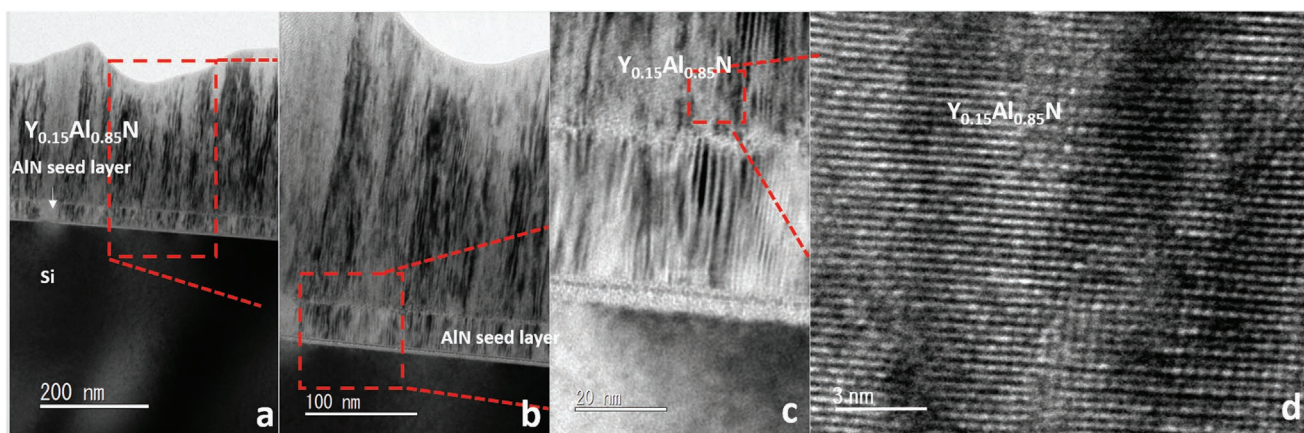


**Figure 6.** Position-dependent, high-resolution transmission electron microscopy (HR-TEM) analysis of the AY sample.

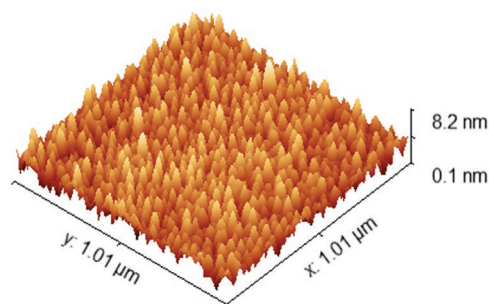


**Figure 7.** 3D representation of the AY sample surface topography by AFM imaging.

of the Y sample, confirmed by the microstructural characterization reported above. In contrast, the AY sample shows a consistent value of  $d_{33}$  of  $785 \text{ pC N}^{-1}$  with precision  $\pm 2\%$  of the measured value, which is in excellent agreement with the predictions mentioned above. As these films are deposited onto a substrate and thus subject to clamping effects, this measured value is an effective value and not the true  $d_{33}$  of  $\text{Y}_{0.15}\text{Al}_{0.85}\text{N}$  film. It is limited by mechanical compliances and the transverse piezoelectric coefficient ( $d_{31}$ ).<sup>[35]</sup> Therefore, it can be concluded that the measured value of  $785 \text{ pC N}^{-1}$  is an underestimated value of the true piezoelectric coefficient ( $d_{33}$ ) of  $\text{Y}_{0.15}\text{Al}_{0.85}\text{N}$ . Akiyama et al.,<sup>[14]</sup> reported a  $d_{33}$  of  $\approx 8 \text{ pC N}^{-1}$  for scandium-alloyed with AlN at an alloying level of 15 at%.

This shows that the inclusion of an AlN seed layer before the deposition of  $\text{Y}_{0.15}\text{Al}_{0.85}\text{N}$  promotes the growth of a highly *c*-axis oriented  $\text{Y}_{0.15}\text{Al}_{0.85}\text{N}$  thin film. The AlN layer provides a crystalline structure, which is similar to YAlN. If the AlN seed layer has a high degree of *c*-axis orientation, then the Y, Al, and N atoms will correctly arrange themselves during film growth in a way to continue the lattice, as it would induce more lattice mismatch-related stress if YAlN would grow in a different crystallographic orientation. As the surface of the AlN seed layer is not exposed to air, it is reasonable to assume that many surface bonds are not saturated, thus improving the nucleation, as these dangling bonds will readily form new bonds with the impinging Y, Al, and N atoms.

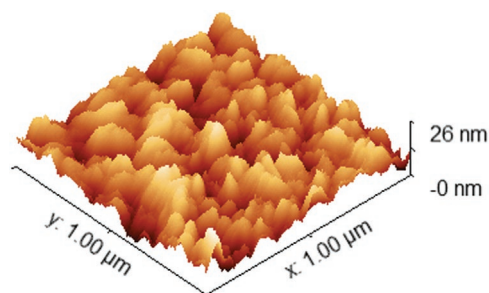


**Figure 8.** 3D representation of the Y sample surface topography by AFM imaging.

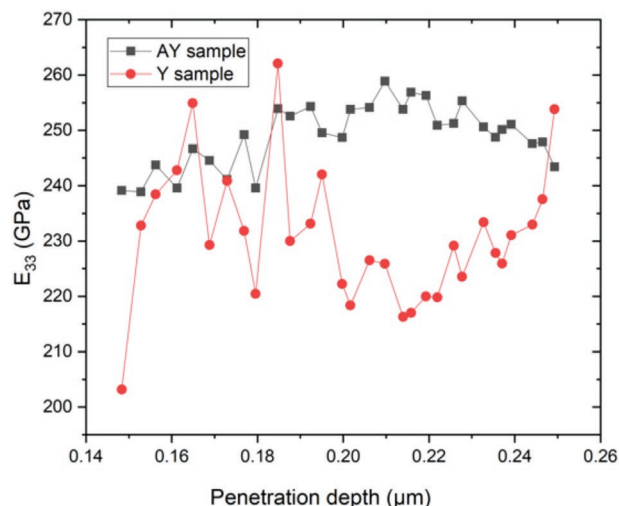


**Figure 9.** Nano-indentation of the Y sample and the AY sample.

## 5. Conclusions

In this study, we have successfully demonstrated the strong impact of AlN as a seed layer on the graining, crystalline quality, and piezoelectric properties of  $\text{Y}_{0.15}\text{Al}_{0.85}\text{N}$  thin films. In addition, high-temperature in situ XRD measurements demonstrate only a slight decrease of oxidation resistance of  $\text{Y}_{0.15}\text{Al}_{0.85}\text{N}$  in a 100% oxygen environment compared to pure AlN, thus offering high stability up to  $800 \text{ }^\circ\text{C}$ . The piezoelectric constant  $d_{33}$  for the  $\text{Y}_{0.15}\text{Al}_{0.85}\text{N}$  thin film with the seed layer is  $785 \text{ pC N}^{-1}$ , and the Young's modulus is  $249 \pm 5.66 \text{ GPa}$ . Both quantities are in excellent agreement with theoretical DFT-based predictions. Future activities will focus on the realization and evaluation of sputter-deposited YAlN thin films with an even higher concentration of yttrium. But, all in all, based on these most promising results,  $\text{Y}_{0.15}\text{Al}_{0.85}\text{N}$  thin films grown on an AlN seed layer offer an excellent potential to replace AlN and even scandium alloyed with AlN as functional material in future silicon MEMS applications, such as sensors, actuators, or high-frequency filter elements.

## Acknowledgements

The authors are thankful to Werner Artner for sharing his experimental knowledge during the high-temperature XRD measurements. This work was supported by the COMET Centre ASSIC Austrian Smart Systems Integration Research Center funded by BMVIT, BMDW, and the Austrian provinces of Carinthia and Styria, within the framework of COMET – Competence Centres for Excellent Technologies. The COMET programme is run by FFG.

## Conflict of Interest

The authors declare no conflict of interest.

## Data Availability Statement

The data that support the findings of this study are available from the corresponding author upon reasonable request.

## Keywords

microelectromechanical systems, piezoelectric, seed layer, thin-film, yttrium aluminum nitride

Received: July 15, 2022

Revised: November 2, 2022

Published online:

- [1] G. Piazza, V. Felmetzger, P. Mural, R. H. Olsson Iii, R. Ruby, *MRS Bull.* **2012**, 37, 1051.
- [2] Y. Liu, Y. Cai, Yi Zhang, A. Tovstopyat, S. Liu, C. Sun, *Micromachines* **2020**, 11, 630.
- [3] A. Gao, K. Liu, J. Liang, T. Wu, *Microsyst. Nanoeng.* **2020**, 6, 74.
- [4] O. Ambacher, *J. Phys. D: Appl. Phys.* **1998**, 31, 2653.
- [5] A. F. Júnior, D. J. Shanafield, *Ceramica* **2004**, 50, 247.
- [6] M. Schneider, A. Bittner, F. Patocka, M. StöGer-Pollach, E. Halwax, U. Schmid, *Appl. Phys. Lett.* **2012**, 101, 221602.
- [7] H. Noma, E. Ushijima, Y. Ooishi, M. Akiyama, N. Miyoshi, K. Kishi, T. Tabaru, I. Ohshima, A. Kakami, T. Kamoharain, *Adv. Mater. Res.*, **2006**, 13–14, 111.
- [8] J. Toledo, V. C. Ruiz-DÁez, M. Bertke, H. Suryo Wasisto, E. Peiner, J. SáNchez-Rojas, *Micromachines* **2019**, 10, 145.
- [9] K. Seo, J. Park, H. Kim, D. Kim, S. Ur, S. Yi, *Integr. Ferroelectr.* **2007**, 95, 74.
- [10] H. Lei, Q. Wen, F. Yu, D. Li, Z. Shang, J. Huang, Z. Wen, *J. Micro-mech. Microeng.* **2018**, 28, 115012.
- [11] V. M. Mastronardi, F. Guido, M. Amato, M. De Vittorio, S. Petroni, *Microelectron. Eng.* **2014**, 121, 59.
- [12] R. Elfrink, T. M. Kamel, M. Goedbloed, S. Matova, D. Hohlfeld, Y. Van Andel, R. Van Schaijk, *J. Micromech. Microeng.* **2009**, 19, 094005.
- [13] H. P. Loebel, M. Klee, C. Metzmacher, W. Brand, R. Milsom, P. Lok, *Mater. Chem. Phys.* **2003**, 79, 143.
- [14] M. Akiyama, T. Kamohara, K. Kano, A. Teshigahara, Y. Takeuchi, N. Kawahara, *Adv. Mater.* **2009**, 21, 593.
- [15] M. S. A. Lozano, A. Pérez-Campos, M. Reusch, L. Kirste, T. Fuchs, A. Žukauskaitė, Z. Chen, G. F. Iriarte, *Mater. Res. Express* **2018**, 5, 036407.
- [16] S. Mertin, B. Heinz, O. Rattunde, G. Christmann, M.-A. Dubois, S. Nicolay, P. Mural, *Surf. Coat. Technol.* **2018**, 343, 2.
- [17] E. Wistrela, I. Schmied, M. Schneider, M. Gillinger, P. M. Mayrhofer, A. Bittner, U. Schmid, *Thin Solid Films* **2018**, 648, 76.
- [18] T. Yokoyama, Y. Iwazaki, Y. Onda, T. Nishihara, Y. Sasajima, M. Ueda, *IEEE Trans. Ultrason. Ferroelectr. Freq. Control* **2015**, 62, 1007.
- [19] M. Uehara, H. Shigemoto, Y. Fujio, T. Nagase, Y. Aida, K. Umeda, M. Akiyama, *Appl. Phys. Lett.* **2017**, 111, 112901.
- [20] A. Žukauskaitė, C. Tholander, J. Palisaitis, P. O. Å. Persson, V. Darakchieva, N. B. Sedrine, F. TasnáDi, B. R. Alling, J. Birch, L. Hultman, *J. Phys. D: Appl. Phys.* **2012**, 45, 422001.
- [21] C. Tholander, I. A. Abrikosov, L. Hultman, F. TasnáDi, *Phys. Rev. B* **2013**, 87, 094107.
- [22] P. M. Mayrhofer, H. Riedl, H. Euchner, M. StáGer-Pollach, P. H. Mayrhofer, A. Bittner, U. Schmid, *Acta Mater.* **2015**, 100, 81.
- [23] S. Manna, G. L. Brennecke, V. Stevanović, C. V. Ciobanu, *J. Appl. Phys.* **2017**, 122, 105101.
- [24] The Institute for Rare Earths and Metals AG, Current prices of rare earths <https://en.institut-seltene-erden.de/aktuelle-preise-von-seltenen-erden/> (accessed: June 2021).
- [25] M. Schlögl, M. Schneider, U. Schmid, *Mater. Sci. Eng., B* **2022**, 276, 115543.
- [26] K. M. Howell, W. Bashir, A. De Pastina, R. Matloub, P. Mural, L. G. Villanueva, *J. Vac. Sci. Technol., A* **2019**, 37, 021504.
- [27] J. Su, S. Fichtner, M. Z. Ghorri, N. Wolff, M. R. Islam, A. Lotnyk, D. Kaden, F. Niekiehl, L. Kienle, B. Wagner, F. Lofink, *Micromachines* **2022**, 13, 783.
- [28] F. Parsapour, V. Pashchenko, S. Mertin, C. Sandu, N. Kurz, P. Nicolay, P. Mural, in *2017 IEEE Int. Ultrasonics Symp. (IUS)*, IEEE, Piscataway, NJ **2017**.
- [29] T. H. Okabe, T. N. Deura, T. Oishi, K. Ono, D. R. Sadoway, *J. Alloys Compd.* **1996**, 237, 150.
- [30] H. Iwanaga, A. Kunishige, S. Takeuchi, *J. Mater. Sci.* **2000**, 35, 2451.
- [31] M. Gillinger, T. Knobloch, A. Marković, G. Pfusterschmied, M. Schneider, U. Schmid, *Mater. Sci. Semicond. Process.* **2018**, 81, 1.
- [32] E. Österlund, G. Ross, M. A. Caro, M. Paulasto-KröCkel, A. Hollmann, M. Klaus, M. Meixner, C. Genzel, P. Koppinen, T. Pensala, A. Žukauskaitė, M. Trebala, *Phys. Rev. Mater.* **2021**, 5, 035001.
- [33] N. Wolff, M. R. Islam, L. Kirste, S. Fichtner, F. Lofink, A. Žukauskaitė, L. Kienle, *Micromachines* **2022**, 13, 1282.
- [34] M. Akiyama, K. Kano, A. Teshigahara, *Appl. Phys. Lett.* **2009**, 95, 162107.
- [35] M. Stewart, M. G. Cain, in *Characterisation of Ferroelectric Bulk Materials and Thin Films*, Springer, Berlin **2014**, pp. 37–64.